

# Ion-atom cold collision: Formation of cold molecular ion by radiative processes

Arpita Rakshit<sup>1</sup> and Bimalendu Deb<sup>1,2</sup>

<sup>1</sup>Department of Materials Science, and <sup>2</sup>Raman Center for Atomic, Molecular and Optical Sciences, Indian Association for the Cultivation of Science, Jadavpur, Kolkata 700032, India.

We discuss theoretically ion-atom collisions at low energy and predict the possibility of formation of cold molecular ion by photoassociation. We present results on radiative homo- and hetero-nuclear atom-ion cold collisions that reveal threshold behaviour of atom-ion systems.

PACS numbers: 34.10.+x, 34.70.+e, 34.50.Cx, 42.50.Ct

## 1. INTRODUCTION

Molecular ions are important for a variety of fundamental studies in physics. For instance, it is proposed that cold molecular ions would be useful for measuring electron dipole moment (EDM) [1, 2]. Study of cold molecular ions has relevance in diverse areas such as metrology [3, 4] and astrochemistry [5]. Recently, molecular ions are cooled into ro-vibrational ground states by all optical [6], laser and sympathetic cooling methods [7, 8]. A large variety of diatomic and triatomic molecular ions are also cooled by sympathetic method [9–11]. Other methods such as photoassociative ionisation [12–16], buffer gas [17], and rotational cooling [18] have been widely used for producing low energy molecular ions. Since cooling of neutral atoms and atomic ions down to sub-milliKelvin temperature regime is possible with currently available technology of laser cooling, it is now natural to ask ourselves: Is it possible to form cold molecular ion by atom-ion cold collision? Recent progress in developing hybrid traps [19–22] where both atomic ions and neutral atoms can be simultaneously confined provides new opportunity for exploring ion-atom quantum dynamics and charge transfer reactions at ultralow

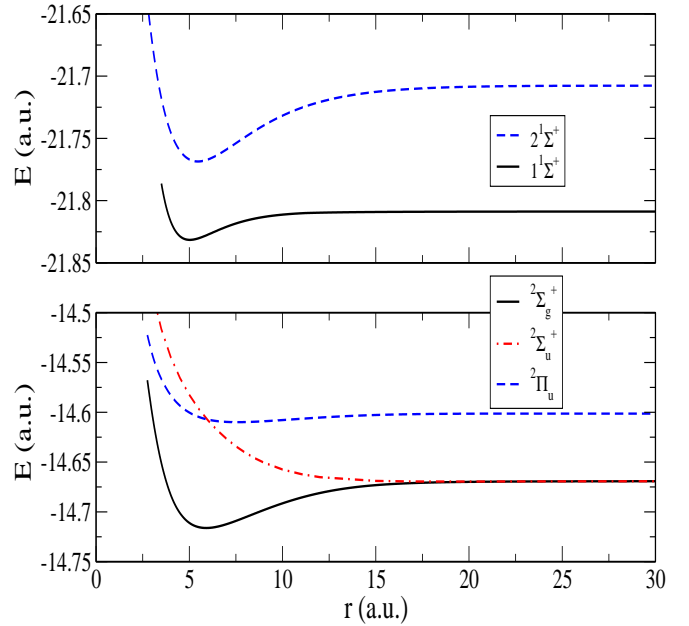


FIG. 2: (Color online) Upper panel shows  $1^1\Sigma^+$  (solid) and  $2^1\Sigma^+$  (dashed) model potentials of  $(\text{LiBe})^+$  system. Lower panel shows  $2^2\Sigma_g^+$  (solid),  $2^2\Sigma_u^+$  (dashed-dotted) and  $2^2\Pi_u$  (dashed) potentials of  $\text{Li}_2^+$ .

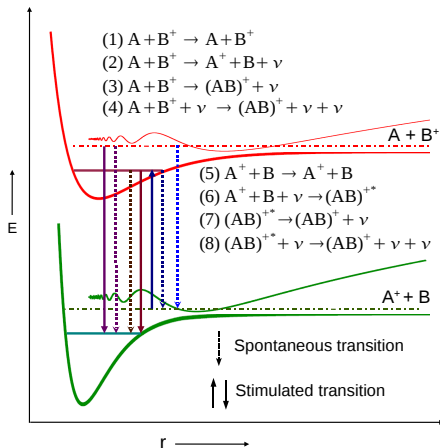


FIG. 1: (Color online) Schematic diagram of possible physical processes which can take place during atom-ion collision at low energy.

temperatures. As neutral cold atoms can be photoassociated [23] into cold dimers, the same association method should also apply to atoms colliding with atomic ions forming cold molecular ions. Understanding ion-atom cold collision [20–22, 24–32] is important for realizing a charged quantum gas, studying charge transport [33] at low temperature, exploring polaron physics [34–36] and producing ion-atom bound-states [37] and cold molecular ions [6–8].

Although in recent times there have been several studies on ion-atom cold collisions, formation of molecular ion by photoassociation (PA) is yet to be demonstrated. There are qualitative differences between atom-atom and ion-atom PA. In contrast to atom-atom PA, hetero-nuclear atom-ion PA is accompanied by charge transfer. Neutral atom-atom PA involves excited diatomic molecular states which in the separated-atom limit correspond of one ground (S) atom and the other excited (P) atom. Hetero-nuclear atom-ion PA may involve excited molecu-

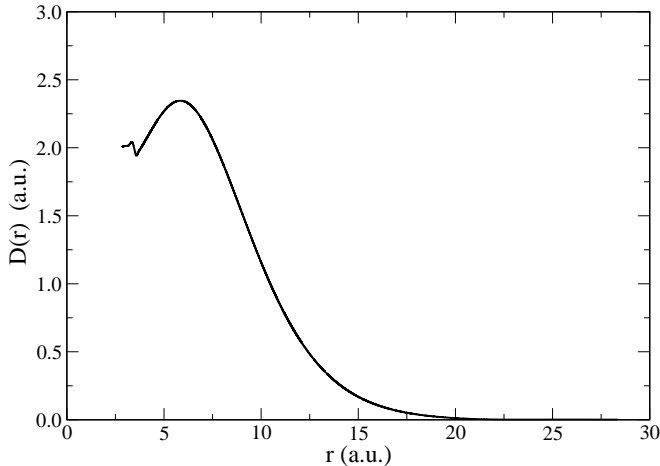


FIG. 3: Radial transition dipole matrix element as a function of separation  $r$  for  $(\text{LiBe})^+$  system.

lar states which asymptotically correspond to separated atom and ion both belonging to S electronic states. The long-range potentials of ion-atom system behave quite differently from those of neutral atom-atom system.

Here we show that it is possible to form translationally and rotationally cold molecular ion by PA. We specifically focus on hetero-nuclear radiative processes. However, we study in general both homo- and hetero-nuclear ion-atom cold collisions to reveal the contrast between the two processes. At ultralow collision energies, radiative charge transfer processes dominate over non-radiative ones. Starting from a cold alkaline metal earth ion and an ultracold alkali atom (such as an atom of alkali Bose-Einstein condensates) as the initial reactants, formation of ground state molecular ion requires a three-step radiative reaction process. In the first step, the ion-atom pair in the continuum of the excited electronic state undergoes radiative charge transfer to the continuum of the ground electronic state. In the second step, the ground continuum ion-atom pair is exposed to laser radiation of appropriate frequency to photoassociate them into excited molecular ion. In the third and final step, another laser is used to stimulate the excited molecular ion to deexcite into a particular rovibrational level of ground electronic state. Since molecular ion is formed from initially cold atom and ion, the molecular ion remains translationally and rotationally cold. One noteworthy feature of this method is the selectivity of low lying rotational level. We present selective results on elastic and radiative charge transfer scattering cross sections for both homo- and hetero-nuclear ion-atom collisions. For model potentials of  $(\text{LiBe})^+$  system, we calculate the PA rate of formation of  $\text{LiBe}^+$  molecular ion.

This paper is organised in the following way. In Sec.2, we describe our model focussing on possible elastic and inelastic processes. Results are presented and discussed in Sec.3. In the last section we draw our conclusions.

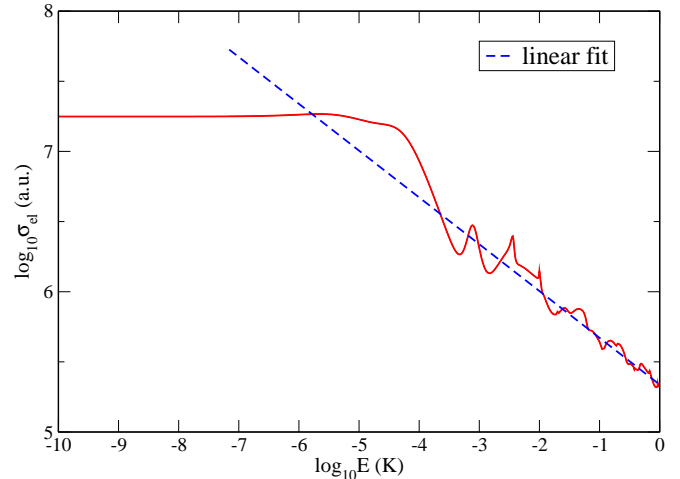


FIG. 4: (Color online) Total elastic scattering cross-section  $\sigma_{el}$  for  $\text{Li} + \text{Be}^+$  ( $2^1\Sigma^+$ ) collision is plotted against collision energy  $E$  in K. The dashed curve is a linear fit for energies greater than  $10^{-6}$  K.

TABLE I: Dissociation energies  $D_e$  in a.u., equilibrium positions  $r_e$  and the effective lengths  $\beta_4$  in Bohr radius for excited and ground state potentials ( $V(r)$ ) of  $(\text{LiBe})^+$  and  $(\text{LiLi})^+$  systems.

system	$V(r)$	$D_e$	$r_e$	$\beta_4$
$(\text{LiBe})^+$	$2^1\Sigma^+$	0.06	5.46	1083.4
$(\text{LiLi})^+$	$2^1\Pi_u$	0.01	7.50	1019.8
$(\text{LiBe})^+$	$1^1\Sigma^+$	0.02	5.03	515.9
$(\text{LiLi})^+$	$2^1\Sigma_g^+$	0.05	6.00	1019.8

## 2. ELASTIC AND INELASTIC PROCESSES

We consider cold collision of an alkali atom A with an alkaline earth metal ion  $B^+$  in a hybrid trap. The possible elastic and inelastic processes are schematically depicted in Fig. 1. These are : (1) elastic collision between A and  $B^+$ , (2) an  $e^-$  from A may hop to  $B^+$  provided they are close enough to each other forming ground state pair of ion  $A^+$  and atom B, (3) atom-ion pair in the excited continuum may decay spontaneously to a bound level of lower electronic state, (4) excited atom-ion pair may be transferred to a ground electronic bound state by stimulated emission process, (5) the ground state atom-ion pair may undergo elastic collision, (6) the ground pair may be photoassociated in the presence of appropriate laser radiation to form excited molecular ion, (7) this excited molecular ion may decay spontaneously either to a ground bound state or continuum, (8) excited bound state may be transferred to a ground bound state by stimulated emission process.

To illustrate atom-ion radiative cold collisions, we consider a model system of  $^7\text{Li} + \text{Be}^+$  undergoing elastic and radiative charge transfer collisions. The possible experimental situation can be imagined as a single  $\text{Be}^+$  ion

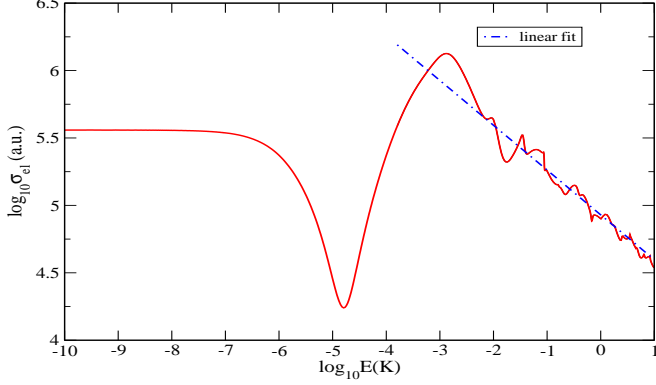


FIG. 5: (Color online) Same as in Fig.4 but for  $\text{Li}^+ + \text{Be}$  ( $1^1\Sigma^+$ ).

immersed in a Bose-Einstein condensate of  $^7\text{Li}$  atoms in a hybrid trap. The molecular potentials  $1^1\Sigma^+$  (ground) and  $2^1\Sigma^+$  (excited) of  $(\text{LiBe})^+$  system as shown in Fig.2 (upper inset) asymptotically go to  $1\text{S} + 1\text{S}$  ( $\text{Li}^+ + \text{Be}$ ) and  $2\text{S} + 2\text{S}$  ( $\text{Be}^+ + \text{Li}$ ), respectively. We construct model potentials  $1^1\Sigma^+$  (ground) and  $2^1\Sigma^+$  (excited) of  $(\text{LiBe})^+$  system using spectroscopic constants given in Ref.[38]. Short range potential is approximated using Morse potential and the long range potential [30, 31] is given by the expression

$$V(r) = -\frac{1}{2} \left( \frac{C_4}{r^4} + \frac{C_6}{r^6} + \dots \right) \quad (1)$$

where  $C_4$ ,  $C_6$  correspond to dipole, quadrupole polarisabilities of atom concerned. The polarisation interaction falls off much more slowly than van der Waals interaction which represents the long range part of interaction between neutral atoms. Hence collision between atom and ion is dominated by the long range polarization interaction. The qualitative feature of this long range interaction of atom-ion is governed by effective length which is given by  $\beta_4 = \sqrt{2\mu C_4/\hbar^2}$  where  $\mu$  is the reduced mass. The short range and long range parts of the potentials are smoothly joined by spline.

Since  $\text{Li}^+$  may be formed due to charge transfer collision between  $\text{Be}^+$  and  $\text{Li}$ , we need to consider the interaction between this  $\text{Li}^+$  and other  $\text{Li}$  atoms present in the condensate. The data for  $2^2\Sigma_g^+$ ,  $2^2\Sigma_u^+$  and  $2^2\Pi_u$  potentials of  $\text{Li}_2^+$  are taken from Ref.[39]. Dissociation energy  $D_e$ , equilibrium position  $r_e$  and effective range  $\beta_4$  of the ground and excited state potentials of  $(\text{LiBe})^+$  and  $\text{LiLi}^+$  systems are given in Table I. A comparison of potentials of these two systems reveals that ground state potential  $1^1\Sigma^+$  of  $(\text{LiBe})^+$  is much shallower than  $2^2\Sigma_g^+$  potential of  $\text{Li}_2^+$ . The equilibrium positions of both ground and excited state potentials of  $(\text{LiBe})^+$  system lie almost at the same separation. Unlike the asymptotic behavior of the excited  $2^1\Sigma^+$  potential of  $(\text{LiBe})^+$  system, the excited state potential  $2^2\Pi_u$  of homonuclear  $\text{Li}_2^+$  molecular ion asymptotically corresponds to one  $\text{Li}^+$

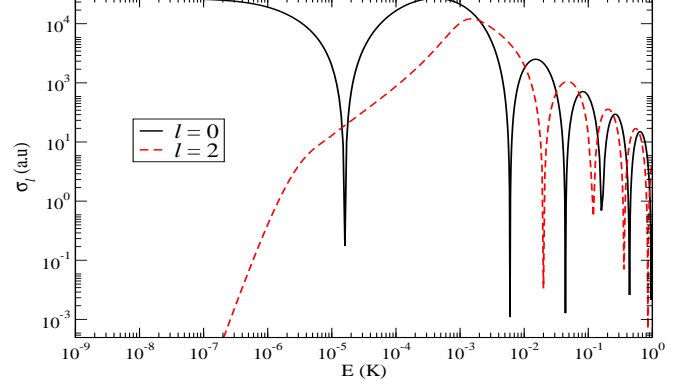


FIG. 6: (Color online) Partial wave cross sections for  $\text{Li}^+ + \text{Be}$  ( $1^1\Sigma^+$ ) collision are plotted as a function of  $E$  (in K) for  $\ell = 0$  (solid) and  $\ell = 2$  (dashed).

ion in the electronic ground S state and one neutral  $\text{Li}$  atom in the excited P state. The equilibrium positions  $r_e$  of ground and excited state potentials of  $\text{Li}_2^+$  system are shifted by 1.5 Bohr radius. For of  $(\text{LiBe})^+$  system, we notice that  $\beta_4$  of excited ( $2^1\Sigma^+$ ) potential is almost twice that of the ground ( $1^1\Sigma^+$ ) potential.

Let us first consider cold collision between  $\text{Li}$  and  $\text{Be}^+$  with both of them being in  $2\text{S}$  electronic state. So, our initial system corresponds to the continuum of  $2^1\Sigma^+$  potential. Due to charge transfer collision neutral  $\text{Be}$  atom and  $\text{Li}^+$  ion are generated. In the separated two-particle limit of this system, dipole transition to ground state at the single particle level is forbidden. Furthermore, since at low energy non-radiative charge transfer is suppressed, the dominant inelastic channel is the radiative charge transfer transition that occurs at intermediate or short separations. Electronic transition dipole moment between two ionic molecular electronic states vanishes at large separation. Therefore, transitions occur at short range where hyperfine interaction is negligible in comparison to central(Coulombic) interaction. The total molecular angular momentum is given by  $\vec{J} = \vec{S} + \vec{L} + \vec{\ell}$  where  $S$  and  $L$  are the total electronic spin and orbital quantum number, respectively; and  $\ell$  stands for the angular quantum number of the relative motion of the two atoms. For the particular model for  $(\text{LiBe})^+$  system chosen here, we have  $L = 0$  and  $S = 0$  for both the ground and the excited electronic states. Thus here the total angular momenta for both the ground and excited states are given by  $J = \ell$ . However, it is more appropriate to denote total angular quantum number of a molecular bound state by  $J$  and that of the continuum or collisional state of this atom-ion system by simply  $\ell$ . The parity selection rule for the electric dipole transition between the ground and excited states dictates  $\Delta J = \pm 1$ .

To investigate ion-atom elastic scattering and free-bound transitions, we need to calculate continuum wave functions which are obtained by solving the partial wave

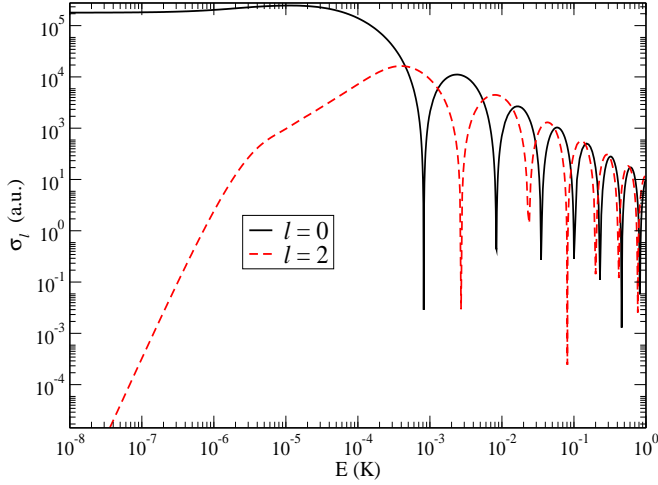


FIG. 7: (Color online) Same as in Fig. 6 but for Li + Li<sup>+</sup> ground state collision in <sup>2</sup>Σ<sub>g</sub> state.

Schrödinger equation given by

$$\left[ \frac{d^2}{dr^2} + k^2 - \frac{2\mu}{\hbar^2} V(r) - \frac{\ell(\ell+1)}{r^2} \right] \psi_\ell(kr) = 0 \quad (2)$$

where  $r$  is the ion-atom separation. The wave function  $\psi_\ell(kr)$  has the asymptotic form  $\psi_\ell(kr) \sim \sin[kr - \ell\pi/2 + \eta_\ell]$  with  $\eta_\ell(k)$  being the phase shift for  $\ell$ -th partial wave. The total elastic scattering cross section is expressed as

$$\sigma_{el} = \frac{4\pi}{k^2} \sum_{\ell=0}^{\infty} (2\ell+1) \sin^2(\eta_\ell) \quad (3)$$

where  $k = \sqrt{2mE/\hbar^2}$ . As the energy gradually increases more and more partial waves start to contribute to total elastic scattering cross sections and the scattering cross section at large energy is [30]

$$\sigma_{el} \sim \pi \left( \frac{\mu C_4^2}{\hbar^2} \right)^{\frac{1}{3}} \left( 1 + \frac{\pi^2}{16} \right) E^{-\frac{1}{3}} \quad (4)$$

As  $k \rightarrow 0$ , according to Wigner threshold laws  $\eta_\ell(k) \sim k^{2\ell+1}$  if  $\ell \leq (n-3)/2$  with  $n$  being the exponent of long-range potential behaving as  $\sim 1/r^n$  as  $r \rightarrow \infty$ . If  $\ell > (n-3)/2$  then the threshold law is  $\eta_\ell(k) \sim k^{n-2}$ . Since the long-range part of ground as well as excited ion-atom potentials goes as  $\sim 1/r^4$  as  $r \rightarrow \infty$ , Wigner threshold laws tell us that s-wave ( $\ell = 0$ ) ion-atom scattering cross section should be independent of  $k$  while all the higher partial wave scattering cross sections should go as  $\sim k^2$  in the limit  $k \rightarrow 0$ .

Ion-atom inelastic collisions are mainly of two kinds - charge transfer reactions and radiative- or photo-associative transfer [40–44]. The radiative charge transfer cross section [40–42] is given by

$$\sigma_{ct} = \int_{\omega_{min}}^{\omega_{max}} \frac{d\sigma_{ct}}{d\omega} d\omega \quad (5)$$

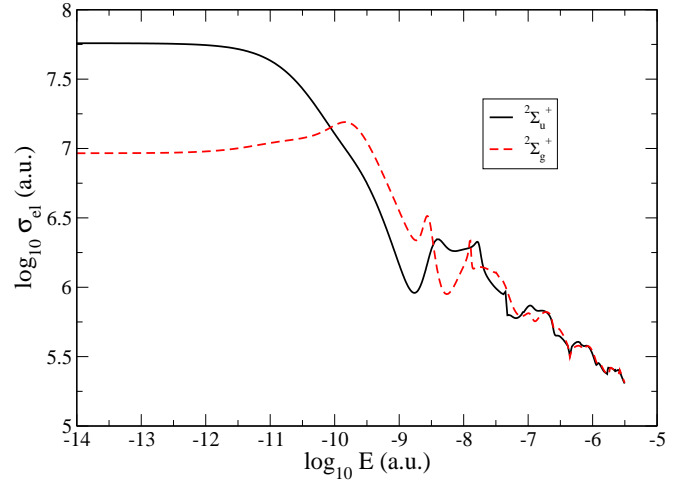


FIG. 8: (Color online) Same as in Fig. 4 but for Li + Li<sup>+</sup> collision in <sup>2</sup>Σ<sub>g</sub><sup>+</sup> (dashed) and <sup>2</sup>Σ<sub>u</sub><sup>+</sup> (solid) potentials.

where  $\omega$  is the angular frequency of emitted photon and

$$\frac{d\sigma_{ct}}{d\omega} = \frac{8\omega^3\pi^2}{3c^3k_m^2} \sum_l [\ell M_{\ell,\ell-1}^2(k_m, k_n) + (\ell+1)M_{\ell,\ell+1}^2(k_m, k_n)] \quad (6)$$

where

$$M_{\ell,\ell'}(k_m, k_n) = \int_0^\infty dr \psi_\ell^m(k_m r) D(r) \psi_{\ell'}^n(k_n r) \quad (7)$$

$D(r)$  is the magnitude of the molecular transition dipole moment. Here  $k_m = \sqrt{2\mu[E - V_m(\infty)]}$  and  $k_n = \sqrt{2\mu[E - V_n(\infty) - \hbar\omega]}$  are the momentum of entrance and exit channels, respectively; and  $E$  is collision energy of entrance ( $m$ ) channel.  $V_m$  and  $V_n$  are the potential energies of the entrance ( $m$ ) and exit ( $n$ ) channels, respectively.  $\psi_\ell^i(k_i r)$  is the wave function of  $\ell$ -th partial wave for  $i$ -th channel of momentum  $k_i$ . The total radiative transfer [41] from the upper state ( $m$ ) to the lower state ( $n$ ) is given by

$$\sigma_{rt} = \frac{\pi}{k_m^2} \sum_{\ell} (2\ell+1) [1 - \exp(-4\zeta_\ell)] \quad (8)$$

where

$$\zeta_\ell = \frac{\pi}{2} \int_0^\infty |\psi_\ell^m(k_m r)|^2 A_{nm}(r) dr \quad (9)$$

is a phase shift and

$$A_{nm}(r) = \frac{4}{3} D^2(r) \frac{|V_n(r) - V_m(r)|^3}{c^3} \quad (10)$$

is the transition probability.

The ground continuum atom-ion pair, formed by radiative charge transfer process, can be photoassociated

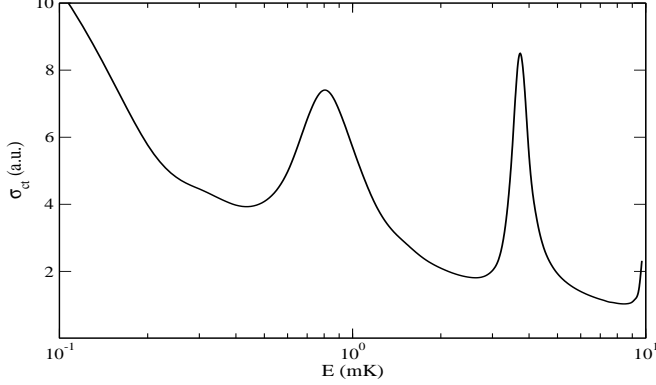


FIG. 9: Charge transfer scattering crosssection  $\sigma_{ct}$  (in a.u.) of  $(\text{LiBe})^+$  system is plotted against collisional energy  $E$  (in mK).

to form excited molecular ion. This process is basically one photon PA process. The photoassociation rate coefficient is given by

$$K_{PA} = \left\langle \frac{\pi v_r}{k^2} \sum_{\ell=0}^{\infty} (2\ell+1) |S_{PA}(E, \ell, w_L)|^2 \right\rangle \quad (11)$$

where  $v_r = \hbar k / \mu$  is the relative velocity of the two particles and  $\langle \dots \rangle$  implies averaging over thermal velocity distribution. Here  $S_{PA}$  is S matrix element given by

$$|S_{PA}|^2 = \frac{\gamma \Gamma_{\ell}}{\delta_E^2 + (\Gamma_{\ell} + \gamma)^2 / 4} \quad (12)$$

where  $\delta_E = E / \hbar + \delta_{vJ}$ ,  $\delta_{vJ} = \omega_L - \omega_{vJ}$  with  $E_{vJ} = \hbar \omega_{vJ}$  being binding energy of the excited ro-vibrational state,  $\omega_L$  being the laser frequency and  $\gamma$  the spontaneous line width. Thus PA rate is primarily determined by partial wave stimulated line width  $\Gamma_{\ell}$  given by

$$\hbar \Gamma_{\ell} = \frac{8\pi^2 I}{3\epsilon_0 c} h(J, \ell) |D_{vJ, \ell}|^2 \quad (13)$$

where

$$D_{vJ, \ell} = \langle \phi_{vJ} | D(r) | \psi_{\ell}(kr) \rangle \quad (14)$$

is the radial transition dipole matrix element between the continuum and bound state wave functions  $\psi_{\ell}(kr)$  and  $\phi_{vJ}(r)$ , respectively.  $I$  is the intensity of laser,  $c$  is the speed of light and  $\epsilon_0$  is the vacuum permittivity. Here  $h(J, \ell)$  is Hönl London factor [45] which in the present context is given by

$$h(J, \ell) = (1 + \delta_{\Lambda'0} + \delta_{\Lambda''0} - 2\delta_{\Lambda'0}\delta_{\Lambda''0}) \frac{1}{(2J+1)(2\ell+1)} \begin{pmatrix} J & 1 & \ell \\ -\Lambda' & \Lambda' - \Lambda'' & \Lambda'' \end{pmatrix}^2 \quad (15)$$

where  $\Lambda'$  and  $\Lambda''$  are the projections of the total electronic orbital angular momentum of the excited and ground

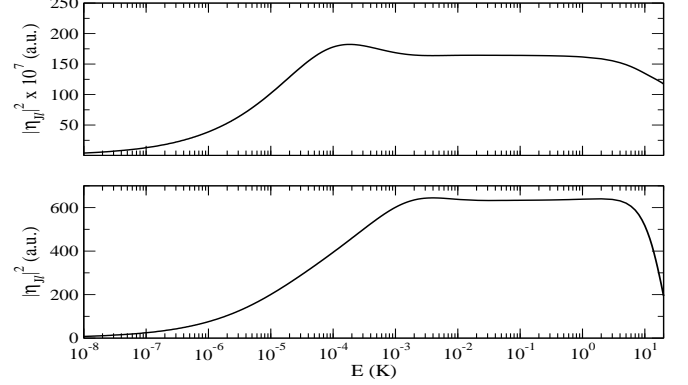


FIG. 10: Square of Franck Condon overlap integral  $|\eta_{J\ell}|^2$  (in a.u.) for  $\text{Li-Li}^+$  (upper) and  $(\text{LiBe})^+$  (lower) is plotted against  $E$  (in K). In the upper panel,  $|\eta_{J\ell}|^2$  is multiplied by a factor of  $10^7$ .

states, respectively, on molecular axis and  $(\dots)$  is the Wigner 3j symbol. The spontaneous line width  $\gamma$  of the excited state  $(v, J)$  is given by

$$\hbar \gamma = \frac{1}{3\pi \epsilon_0 c^3} \left[ \int (\Delta E)^3 |\langle \phi_{vJ} | D(r) | \psi_E \rangle|^2 dE + \sum_{v', J'} \Delta_{v'J'}^3 |\langle \phi_{vJ} | D(r) | \phi_{v'J'} \rangle|^2 \right] \quad (16)$$

where  $\Delta E = (E_{vJ} - E) / \hbar$ ,  $\Delta_{v'J'} = (E_{vJ} - E_{v'J'}) / \hbar$ ,  $\psi_E$  is the scattering wave function and  $|\phi_{v'J'}\rangle$  stands for all the final bound states to which the excited state can decay spontaneously.

### 3. RESULTS AND DISCUSSION

Standard renormalized Numerov-Cooley method [46] is used to calculate the bound and scattering state wave functions. The molecular transition dipole matrix element of  $(\text{LiBe})^+$  system is calculated using GAMESS. This matrix element strongly depends upon separation and goes to zero at a large  $r$  as shown in Fig.3. In Figs. 4 and 5, we have plotted the excited and ground state elastic scattering cross section  $\sigma_{el}$  as a function of energy  $E$  for  $\text{Li} + \text{Be}^+$  and  $\text{Li}^+ + \text{Be}$  collisions, respectively. We find that at least 35 partial waves are required to get converging results on elastic scattering for energies higher than  $1 \mu\text{K}$ . In our calculations we have used 51 partial waves. At high energies, for both the cases,  $\sigma_{el}$  decreases as  $E^{-\frac{1}{3}}$ . The proportionality constant  $c$  in the expression  $\sigma_{el}(E \rightarrow \infty) = cE^{-\frac{1}{3}}$  calculated using Eq. (4) for excited  $2^1\Sigma^+$  and ground  $1^1\Sigma^+$  potentials are 2936 and 1091 a.u., respectively, whereas linear fit to  $\sigma_{el}$  vs.  $E$  curves provides  $c = 3548$  and  $1335$  a.u., respectively. Figures 6 and 7 exhibit s- and d-wave partial scattering cross section as a function of energy for  $\text{Li}^+ + \text{Be}$  and  $\text{Li} + \text{Li}^+$  collisions, respectively. These figures show that

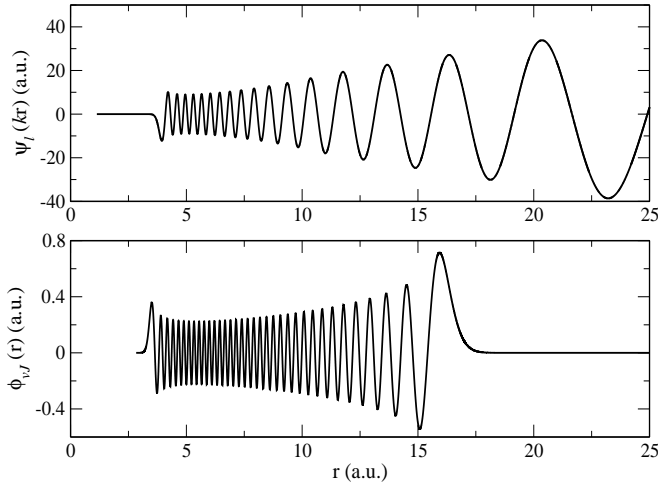


FIG. 11: Energy-normalized s-wave ground scattering (upper) and unit normalized excited bound (lower) wave functions of  $(\text{LiBe})^+$  system are plotted as a function of separation  $r$ .

the Wigner threshold behavior begins to set in as the collision energy decreases below  $0.1 \mu\text{K}$ . In Fig. 8, we have plotted total elastic scattering cross section for  $\text{Li}+\text{Li}^+$  collisions in  $^2\Sigma_g^+$  and  $^2\Sigma_u^+$  potentials.

Starting from the low energy continuum state of  $\text{Li} + \text{Be}^+$  collision in the  $2^1\Sigma^+$  potential, there arise two possible radiative transitions by which the system can go to the ground electronic state  $1^1\Sigma^+$ . One is continuum-continuum and the other is continuum-bound dipole transition. The transition dipole moment as a function of separation as shown in Fig. 3 shows that the dipole transition probability will vanish as the separation increases above  $20a_0$ . So, a dipole transition has to take place at short separations. Let us consider radiative transfer processes from the upper ( $2^1\Sigma^+$ ) to the lower ( $1^1\Sigma^+$ ) state of  $(\text{LiBe})^+$ . We then need to apply the formulae (5) and (8) where  $m \equiv 2^1\Sigma^+$  and  $n \equiv 1^1\Sigma^+$  in our case. Continuum-continuum charge transfer cross section  $\sigma_{ct}$  between  $2^1\Sigma^+$  and  $1^1\Sigma^+$  states of  $(\text{LiBe})^+$  system is plotted against  $E$  in Fig.9. We evaluate the photoassociative (continuum-bound) transfer cross section by subtracting  $\sigma_{ct}$  from the total radiative transfer cross section  $\sigma_{rt}$  calculated using the formula (8). At energy  $E = 0.1 \text{ mK}$ ,  $\sigma_{ct}$  and the photoassociative transfer cross section are found to be  $10.39 \text{ a.u.}$  and  $0.03 \text{ a.u.}$ , respectively. Thus we infer that the continuum-continuum radiative charge transfer process dominates over the radiative association process. Also, we notice that  $\sigma_{ct}$  is smaller than both the excited and ground state elastic scattering cross sections  $\sigma_{el}$  (as given in Fig.4 and 5, respectively) by several orders of magnitude.

Molecular dipole transitions between two ro-vibrational states or between continuum and bound states are governed by Franck-Condon principle. According to this principle, for excited vibrational (bound) states, bound-bound or continuum-bound transitions

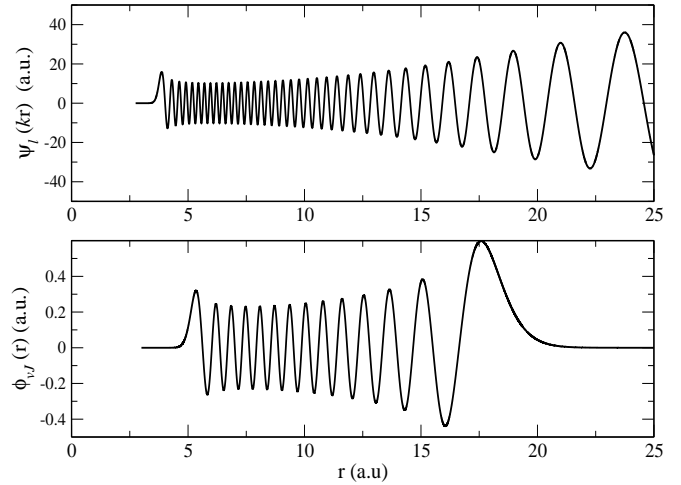


FIG. 12: Same as in Fig.11 but for  $\text{Li-Li}^+$  system.

primarily occur near the turning points of bound states. In general, highly excited vibrational state wave functions of diatomic molecules or molecular ions have their maximum amplitude near the outer turning points. Spectral intensity is proportional to the overlap integral. This means that the spectral intensity for a continuum-bound transition would be significant when the continuum state has a prominent node near the outer turning point of the bound state. For transitions between two highly excited bound states, Franck-Condon principle implies that the probability of such transitions would be significant when the outer turning points of these two bound states lie nearly at the same separation. The upper panel of Fig.10 shows the variation of the square of Franck-Condon overlap integral  $|\eta_{J\ell}|^2$  between the ground s-wave ( $\ell = 0$ ) scattering and the excited ro-vibrational ( $v = 26, J = 1/2$ ) states of  $\text{Li-Li}^+$  system as a function of the collision energy  $E$ . The lower panel of Fig.10 displays the same as in the upper panel but for  $(\text{LiBe})^+$  system with  $v = 68$  and  $J = 1$ . The excited ro-vibrational state  $v = 26, J = 1/2$  of  $\text{Li-Li}^+$  is very close to dissociation threshold while the excited ro-vibrational state  $v = 68, J = 1$  of  $(\text{LiBe})^+$  system is a deeper bound state. These two excited states are so chosen such that free-bound Franck-Condon overlap integral for both the systems become significant. Comparing these two plots, we find that  $|\eta_{J\ell}|^2$  of  $\text{Li-Li}^+$  system is smaller than that of  $(\text{LiBe})^+$  system by seven orders of magnitude. To understand why the values  $|\eta_{J\ell}|^2$  for the two systems are so different, we plot the energy-normalized s-wave ground scattering and the bound state wave functions of  $(\text{LiBe})^+$  system in Fig.11 and those of  $\text{Li-Li}^+$  system in Fig.12. A comparison of Figs.11 and 12 reveals that, while in the case of  $(\text{LiBe})^+$  the maximum of the excited bound state wave function near the outer turning point coincides nearly with a prominent antinode of the scattering wave function, in the case of  $\text{Li-Li}^+$  the maximum of the bound state wave function near the outer turning point almost coincides with a minimum

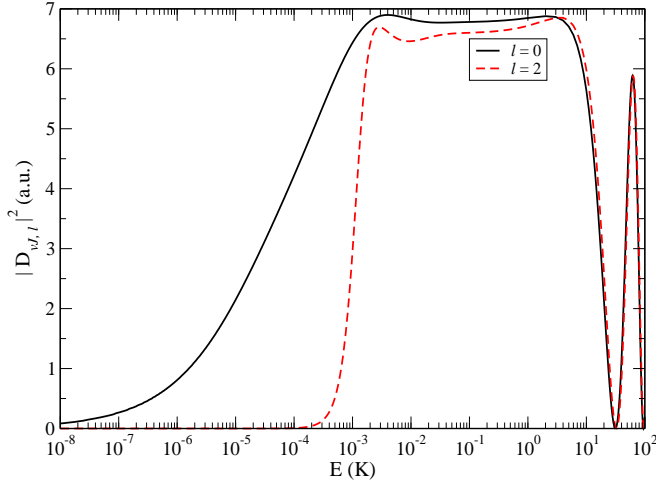


FIG. 13: (Color online) Square of free-bound radial transition dipole moment ( $|D_{vJ,l}|^2$ ) (in a.u.) for ground continuum states with  $\ell = 0$  (solid) and  $\ell = 2$  (dashed) and excited bound ro-vibrational level with  $v = 68$  and  $J = 1$

TABLE II: Ro-vibrational energy ( $E_{vJ}$ ), inner ( $r_i$ ) and outer turning points ( $r_o$ ) of two selected bound states of  $(\text{LiBe})^+$  molecular ion - one bound state in excited ( $2^1\Sigma^+$ ) and the other in ground ( $1^1\Sigma^+$ ) potential. The energy  $E_{vJ}$  is measured from the threshold of the respective potential.

Potential	$v$	$J$	$E_{vJ}$ (a.u.)	$r_i$ (a.u.)	$r_o$ (a.u.)
$2^1\Sigma^+$	68	1	$-3.30 \times 10^{-3}$	3.4	16.3
$1^1\Sigma^+$	29	0	$-0.25 \times 10^{-3}$	3.8	16.6

(node) of the scattering wave function. These results indicate that the possibility of the formation of excited  $\text{LiLi}^+$  molecular ion via PA is much smaller than that of  $(\text{LiBe})^+$  ion. We henceforth concentrate on PA of  $(\text{LiBe})^+$  system only.

We next explore the possibility of PA in  $\text{Li}^+$ -Be cold collision in the presence of laser light. As discussed before, continuum-bound molecular dipole transition matrix element depends on the degree of overlap between continuum and bound states. PA rate (11) is proportional to the square of free-bound radial transition dipole moment element  $|D_{vJ,l}|^2$ . In Fig. 13 we plot  $|D_{vJ,l}|^2$  against  $E$  for s- ( $\ell = 0$ ) and d-wave ( $\ell = 2$ ) ground scattering states and  $v = 68$ ,  $J = 1$  excited molecular state. It is clear from this figure that the contributions of both  $\ell = 0$  and  $\ell = 2$  partial waves are comparable above energy corresponding to 0.1 mK. At lower energy ( $E < 0.1$  mK), only s-wave makes finite contribution to the the dipole transition. Figure 14 exhibits  $|D_{vJ,l}|^2$  as a function of  $E$  for the transition from s-wave ( $\ell = 0$ ) scattering state of the excited ( $2^1\Sigma^+$ ) continuum to the ground ( $1^1\Sigma^+$ ) ro-vibrational state with  $v = 36$ ,  $J = 1$ . A comparison between the Figs.13 and 14 reveals that the probability for the transition from the upper continuum to the ground bound state is smaller by several orders of magnitude than that from ground continuum to an ex-

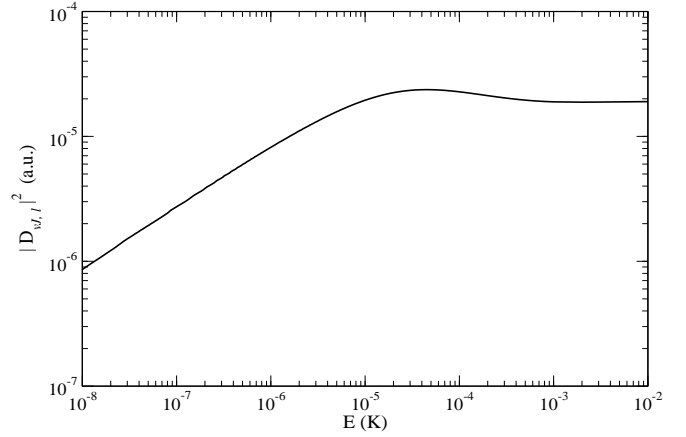


FIG. 14: Same as in Fig.13 but for excited continuum state with  $\ell = 0$  and ground ro-vibrational state with  $v = 36$  and  $J = 1$ .

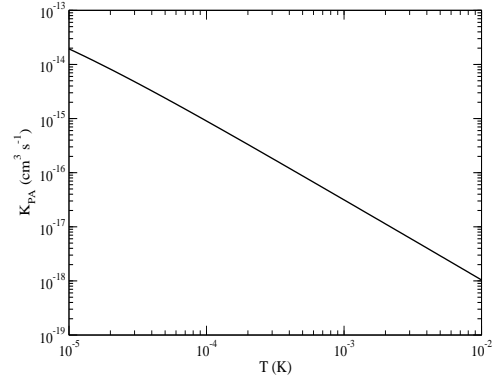


FIG. 15: Rate of photoassociation  $K_{PA}$  (in  $\text{cm}^3 \text{s}^{-1}$ ) of  $(\text{LiBe})^+$  is plotted against temperature (in K) at  $I = 1 \text{ W/cm}^2$  and  $\delta_{vJ} = \omega_L - \omega_{vJ} = 0$

cited bound state. In Fig 15, we have plotted the rate of photoassociation  $K_{PA}$  as a function of temperature  $T$  for laser frequency tuned at PA resonance. The ion-atom PA rate as depicted in Fig.15 is comparable to the typical values of rate of neutral atom-atom PA at low laser intensities. In Fig. 16 we have plotted the rate of photoassociation as a function of laser intensity at a fixed temperature  $T = 0.1$  mK to show the saturation effect that occurs around intensity  $I = 50 \text{ kW/cm}^2$ . Thus the formation of excited  $(\text{LiBe})^+$  molecular ion by photoassociating colliding  $\text{Li}^+$  with Be with a laser of moderate intensity appears to be a feasible process.

Now we discuss the possibility of formation of ground state molecular ion by stimulated Raman-type process by applying a second laser tuned near a bound-bound transition between the excited and ground potentials. Let us consider two selected bound states whose salient features are given in Table-II. The outer turning points of these two bound states almost coincide implying the existence of a large Franck-Condon overlap between them. To see whether coherent laser coupling between these two bound



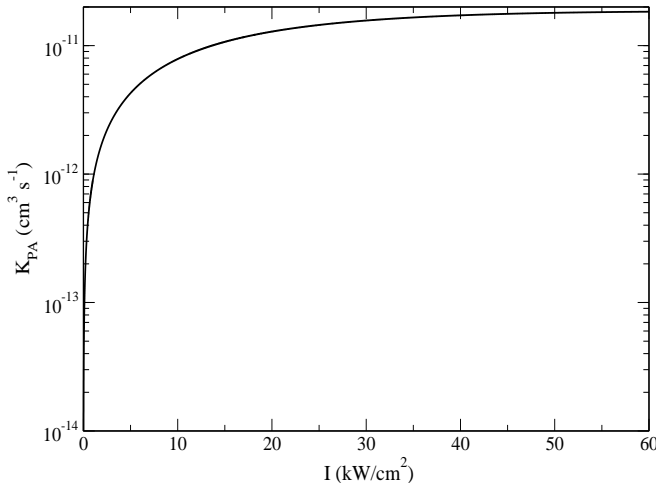


FIG. 16:  $K_{PA}$  (in  $\text{cm}^3 \text{s}^{-1}$ ) of  $(\text{LiBe})^+$  is plotted as a function of laser intensity  $I$  (in  $\text{kW}/\text{cm}^2$ ) at temperature  $T = 0.1$  mK with laser tuned at PA resonance.

states is possible or not, we calculate Rabi frequency  $\Omega$  given by

$$\hbar\Omega = \left( \frac{I}{4\pi c\epsilon_0} \right)^{\frac{1}{2}} |\langle v, J | \vec{D}(r) \cdot \hat{\epsilon}_L | v', J' \rangle| \quad (17)$$

where  $\hat{\epsilon}_L$  is the unit vector of laser polarization and  $|v, J\rangle$  and  $|v', J'\rangle$  are the two bound states with  $\langle r | v, J \rangle = \phi_{vJ}(r)$ . Rabi frequency corresponding to this bound-bound transition is found to be 285 MHz for laser intensity  $I = 1 \text{ kW}/\text{cm}^2$ . Comparing this value with the spontaneous line width  $\gamma = 57 \text{ kHz}$  of the excited bound state calculated using the formula (16), we infer

that even at a low laser intensity which is far below the saturation limit, bound-bound Rabi frequency  $\Omega$  exceeds  $\gamma$  by several orders of magnitude. This indicates that it may be possible to form ground molecular ion by stimulated Raman-type process with two lasers.

#### 4. CONCLUSION

In conclusion, we have shown that alkaline earth metal ions immersed in Bose-Einstein condensates of alkali atoms can give rise to a variety of cold chemical reactions. We have analyzed in detail the elastic and inelastic processes that can occur in a system of a Beryllium ion interacting with cold Lithium atoms. We have predicted the formation of translationally and rotationally cold  $(\text{LiBe})^+$  molecular ion by photoassociation. Theoretical understanding of low energy atom-ion scattering and reactions may be important for probing dynamics of quantum gases. Since both Bose-Einstein condensation and fermionic superfluidity have been realized in atomic gases of Lithium, understanding cold collisions between Lithium and Beryllium ion may be helpful in probing both bosonic and fermionic superfluidity. In particular, this may serve as an important precursor for generating and probing vortex ring in Lithium quantum gases.

#### Acknowledgments

AR is grateful to CSIR, Government of India, for a support. We are thankful to P. Ghosh, Presidency College, Kolkata for his help in computation.

- 
- [1] R. P. Stutz and E. A. Cornell, *Bull. Am. Soc. Phys.* **89**, 76 (2004).
  - [2] E. R. Meyer, J. L. Bohn and M. P. Deskevich, *Phys. Rev. A* **73**, 062108 (2006); E. R. Meyer and J. L. Bohn, *Phys. Rev. A* **78**, 010502(R) (2008); E. R. Meyer and J. L. Bohn, *Phys. Rev. A* **80**, 042508 (2009)
  - [3] J. C. J. Koelemeij, B. Roth, A. Wicht, I. Ernsting and S. Schiller, *Phys. Rev. Lett.* **98**, 173002 (2007)
  - [4] S. Schiller and V. Korobov, *Phys. Rev. A* **71**, 032505 (2005).
  - [5] I. W. M. Smith, *Low Temperature and Cold Molecules* (Imperial College Press, 2008)
  - [6] T. Schneider, B. Roth, H. Duncker, I. Ernsting and S. Schiller, *Nature phys.* **6**, 275 (2010)
  - [7] E. R. Hudson, *Phys. Rev. A* **79**, 032716 (2009)
  - [8] P. F. Staunum, K. Højbjerg, P. S. Skyt, A. K. Hansen and M. Drewsen, *Nat. phys.* **6**, 271 (2010)
  - [9] B. Roth, P. Blythe, H. Daerr, L. Patacchini and S. Schiller, *J. Phys. B: At. Mol. Opt. Phys.* **39**, S1241 (2006); B. Roth, A. Ostendorf, H. Wenz and S. Schiller, *J. Phys. B: At. Mol. Opt. Phys.* **38**, 3673 (2005)
  - [10] A. Ostendorf, C. B. Zhang and M. A. Wilson, D. Ofenberger, B. Roth, and S. Schiller, *Phys. Rev. Lett.* **97**, 243005 (2006)
  - [11] K. Mølhave and M. Drewsen, *Phys. Rev. A* **62**, 011401 (2000)
  - [12] V. S. Bagnato and J. Weiner, P. S. Julienne and C. J. Williams, *Laser Physics* **4**, 1062 (1994)
  - [13] P. L. Gould, P. D. Lett and P. S. Julienne *et al.*, *Phys. Rev. Lett.* **60**, 788 (1988)
  - [14] M. E. Wagshul, K. Helmerson, P. D. Lett *et al.*, *Phys. Rev. Lett.* **70**, 2074 (1993)
  - [15] V. Bagnato, L. Marcassa and C. Tsao *et al.*, *Phys. Rev. Lett.* **70**, 3225 (1993)
  - [16] J. P. Shaffer, W. Chalupczak and N. P. Bigelow, *Phys. Rev. Lett.* **82**, 1124 (1999)
  - [17] J. C. Pearson, L. C. Oesterling, E. Herbst and F. C. De Lucia, *Phys. Rev. Lett.* **75**, 2940 (1995)
  - [18] I. S. Vogelius, L. B. Madsen and M. Drewsen, *Phys. Rev. A* **70**, 053412 (2004); I. S. Vogelius, L. B. Madsen and M. Drewsen *J. Phys. B: At. Mol. Opt. Phys.* **39**, S1267 (2006); K. Højbjerg, A. K. Hansen, P. S. Skyt, P. F. Staunum and M. Drewsen, *New J. Phys.* **11**, 055026 (2009)



- [19] W. W. Smith, O. P. Marakov and J. Lin, *J. of Mod. Opts.* **52**, 2253 (2005)
- [20] C. Zipkes, S. Palzer, C. Sias and M. Kohl, *Nature Lett.* **464**, 388 (2010)
- [21] C. Zipkes, S. Palzer, L. Ratschbacher, C. Sias, and M. Kohl, *arXiv1005:3846v2* (2010)
- [22] A. T. Grier, M. Cetina, F. Oručević, and V. Vuletić, *Phys. Rev. Lett.* **102**, 223201 (2009)
- [23] John Weiner, V. S. Bagnato, S. Zilio and P. S. Julienne, *Rev. Mod. Phys.* **71**, 1 (1999); K. M. Jones, E. Tiesinga, P. D. Lett, and P. S. Julienne, *Rev. Mod. Phys.* **78**, 483 (2006)
- [24] S. Schmid, A. Härter and J. H. Denschlag, *arXiv:1007.4717v1* (2010)
- [25] E. Bodo, P. Zhang and A. Dalgarno, *New J. Phys.* **10** 033024 (2008)
- [26] P. Zhang, E. Bodo and A. Dalgarno, *J. Phys. Chem. A* **113**, 15085 (2009)
- [27] Peng Zhang, Alex Dalgarno, and Robin Côté, *Phys. Rev. A* **80**, 030703(R) (2009)
- [28] Z. Idziaszek, T. Calarco, P. S. Julienne, and A. Simoni, *Phys. Rev. A* **79**, 010702(R) (2009)
- [29] B. Gao, *arXiv:1002.1022v2*
- [30] R. Côté and A. Dalgarno, *Phys. Rev. A* **62**, 012709 (2000)
- [31] O. P. Makarov, R. Côté, H. Michels, and W. W. Smith, *Phys. Rev. A* **67**, 042705 (2003)
- [32] X. Ma, X. L. Zhu and B. Li *et al.*, *J. Phys: Conference Series* **88**, 012019 (2007)
- [33] R. Côté, *Phys. Rev. Lett.* **85**, 5316 (2000)
- [34] P. Massignan, C. J. Pethick, and H. Smith, *Phys. Rev. A* **71**, 023606 (2005).
- [35] R. M. Kalas, and D. Blume, *Phys. Rev. A* **73**, 043608 (2006).
- [36] F. M. Cucchietti, and E. Timmermans, *Phys. Rev. Lett.* **96**, 210401 (2006).
- [37] R. Côté, V. Kharchenko, and M. D. Lukin, *Phys. Rev. Lett.* **89**, 093001 (2002).
- [38] A. A. Safonov, V. F. Khrustov and N. F. Stepanov, *Zhurnal Strukturnoi Khimii* **24**, 168 (1983)
- [39] D. D. Konowalow and M. E. Rosenkrantz, *Chem. Phys. Lett.* **61**, 489 (1979)
- [40] D. L. Cooper, K. Kirby, and A. Dalgarno, *Canadian J. Phys.* **62**, 1622 (1984)
- [41] B. Zygelman and A. Dalgarno, *Phys. Rev. A* **38**, 1877 (1988)
- [42] B. Zygelman, A. Dalgarno, M. Kimura and N. F. Lane, *Phys. Rev. A* **40**, 2340 (1989)
- [43] P. C. Stancil and B. Zygelman, *Astro. J.* **472**, 102 (1996)
- [44] B. W. West, N. F. Lane and J. S. Cohen, *Phys. Rev. A* **26**, 3164 (1982)
- [45] H. R. Thorsheim, J. Weiner, P. S. Julienne, *Phys. Rev. Lett.* **58**, 2420 (1987); A. Hansson and J. K. G. Watson, *J. Mol. Spec.* **233**, 169 (2005)
- [46] B. R. Johnson, *J. Chem. Phys.* **67**, 4086 (1977)